Preprint Title	Enhanced and ultrafast dye contaminated wastewater remediation using molybdenum doped bismuth ferrite nanoparticles
Authors	Sonam Chakraborty and Mrinal Pal
Publication Date	09 Sep 2019
Article Type	Full Research Paper
ORCID® iDs	Mrinal Pal - https://orcid.org/0000-0002-1032-272X

Enhanced and ultrafast dye contaminated wastewater remediation using molybdenum doped bismuth ferrite nanoparticles

Sonam Chakraborty and Mrinal Pal*

CSIR- Central Glass and Ceramic Research Institute, Kolkata – 700032, India

email:sonammana@gmail.com, palm@cgcri.res.in*

Corresponding author's address:

Dr. Mrinal Pal

Division of sensor and actuator,

CSIR - Central Glass and Ceramic Research Institute, Kolkata – 700032, India

Email: palm@cgcri.res.in

Abstract

Industrial effluents containing various dyes are a potential threat to the environment and its remediation has become a challenging task for the scientists.We demonstrated here for the first time the ultrafast and improve dye degradation capability of bismuth ferrite (BFO) nanoparticles by molybdenum doping prepared through a facile chemical route. Phase purity and microstructural characterization of the prepared samples were carried out using thermogravimetric analysis (TGA), X-ray diffraction (XRD), scanning electron microscopy (SEM), transmission electron microscopy (TEM), UV-vis and photoluminescence (PL) spectroscopy. It was observed that doping of molybdenum not only enhance the photocatalytic activity by four-fold of the pristine sample but also make the process very fast. Experimental results delineate that 10 mg/l rhodamine-B (RhB) degrades more than 80% under irradiation of visible light for only 5 min at the ambient condition without using any remarkable promoter. Also it can also degrade other dyes (methylene blue, bismark brown) and the process is almost independent of pH which is good for application purpose. In totality, molybdenum doped BFO nanoparticles could be very good promising candidates for dye degradation to clean industrial effluents quickly through an easy and inexpensive way for the benefit of society.

Keywords

Dye-degradation, Mo-doped BFO, Nanoparticles, Rhodamine B, Ultrafast, Visible light.

1. Introduction

Recently there is a huge increase in the use of organic dyes in different industries e.g. food, textile, pharmaceuticals. These organics dyes are considered to be one of the most common sources of water pollution due to their non-biodegradability and high toxicity level towards a human being and aquatic creatures [1-3]. Therefore, the degradation of these dyes in an eco-friendly and energy efficient manner received widespread attention all over the world. Different materials and techniques were investigated to achieve efficient and fast dye degradation using visible light. Among them, photocatalytic oxidation is considered to be the easier, efficient and low-cost process to degrade these organic dyes under irradiation of UV or visible light [4, 5]. Rhodamine B (RhB) is a highly water-soluble and toxic dye mainly used in textile, paper and pharmaceuticals industries. It causes severe allergy to respiratory organs, skin and eyes. Since it is highly soluble and stable in water it affects the aquatic creatures very badly. Therefore, control over this type of toxic and soluble organic dye is considered to be the most important issue for researchers [6-8].

Bismuth ferrite (BFO) nanoparticles are considered a versatile material with lots of excellent and interesting applications in photovoltaic, solar cell, gas sensing, excellently visible light photocatalysis [9-12]. Since BFO has a moderate band gap (2.2 eV) with a high thermal and chemical stability it can be a potential candidate for photocatalytic dye-degradation using visible light. But due to its high rate of electron-hole recombination it is still not considered to be a well-established photocatalyst. Measures have been taken to increase the recombination time of the electron-hole pair by producing different trapping centres, defects etc in the materials.

There are several reports on the photocatalytic effect of BFO nanoparticles where it has been demonstrated that either doping or by creating different morphologies it is possible to

increases the photocatalytic activity [13, 14]. Zhang et al. have shown an effective enhancement in RhB degradation capability when BFO nanoparticles are doped with Gd^{3+} [15]. A study by Irfan et al. delineates that on co-doping the BFO nanoparticles with Sn^{4+} and Gd^{3+} its photocatalytic property increases [16]. On substitution of Bi^{3+} of BFO with Dy^{3+}Sarkar et al. has shown a remarkable increase in its catalytic activity towards degradation of methyl blue (MB) under UV irradiation [17]. Yang et al. demonstrated that doping of Sr^{2+} on BFO nanoparticle effectively increases the magnetic as well as photocatalytic property [18]. The effect of La^{3+} and Se^{4+} co-doping was investigated by Irfan et al [19]. It was observed that on co-doping the band gap decreases from 2.06 eV–1.94 eV and photocatalytic degradation of congo red effectively increases. Also, there are several reports which confirm that suitable doping will definitely increase the catalytic activity of nanoparticles. Though the dye-degradation capability of BFO was well demonstrated by many groups in all the reports photocatalytic activity is achieved either by using UV light or some promoter likes H_2O_2 which are constrained for real-life application.

Nonetheless, the need of the hour is to design some novel materials/ systems such that degradation of dyes will be made very quickly, inexpensively using simple visible light at ambient condition without any promoter. In this work, we have taken up the challenge and reporting fast and efficient dye degradation capability of BFO nanoparticles towards RhB by doping with Mo. It works under visible light and without any promoter. Prepared Mo-doped BFO nanoparticles can also degrade other dyes (methylene blue, bismark brown) and the process is almost independent of pH.

2. Experiment

2.1 Materials and methods

Bismuth nitrate pentahydrate ($Bi(NO_3)_3.5H_2O$), iron nitrate nonahydrate ($Fe(NO_3)_3.9H_2O$), ammonium heptamolybdatetrahydrate ($(NH_4)_6Mo_7O_{24}\cdot 4H_2O$), tartaric acid ($C_4H_6O_6$), rhodamine b (RhB), methyl blue, bismarck brown were procured from Merck India and used without further purification.

2.2 Synthesis of Mo doped BFO nanoparticles

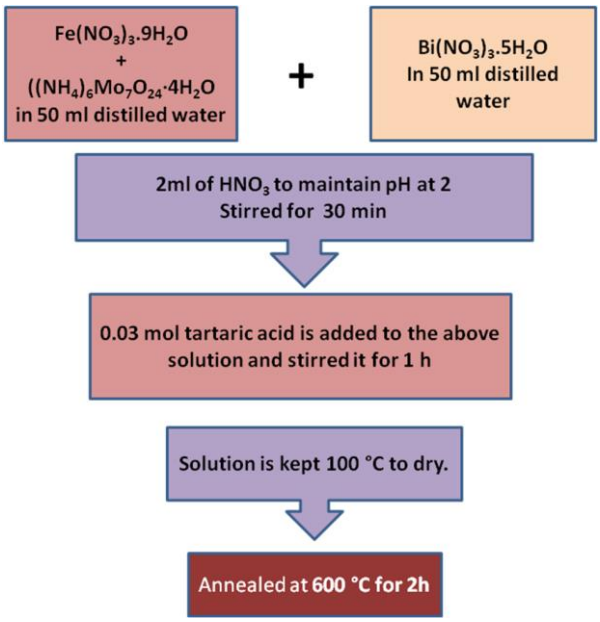

Figure 1 Schematic of synthesis procedure.

Mo-doped BFO nanoparticles ($BiMo_xFe_{1-x}O_3$) where x = 0.0, 0.025, 0.05, 0.075, 0.1 were synthesised by simple sol-gel technique. A solution of 0.015 mol was prepared by taking the required amount of each iron nitrate nonahydrate and ammonium heptamolybdate tetrahydrate together in 50 ml of distilled water. Another solution of 0.015 mol was prepared by mixing of a required amount of bismuth nitrate pentahydrate in 50 ml of distilled water. The second solution was slowly mixed with the first solution under vigorous stirring. 2 ml of HNO_3 (69%) was added in this mixture to maintain the pH at around 2. Again a third solution of 0.05 mol was made by dissolving the required amount of tartaric in 30 ml of distilled water. This third solution was poured slowly into the above mixture and stirred for 1 h. The prepared solution was then put in the hot plate with a constant stirring of 7 h at 100 °C.

Finally, the dried gel was annealed at 600 °C for 2 hours for further used. Schematic of the synthesis procedure is displayed in Figure 1.

2.3 Characterizations

NETZSCH 44C was used to perform thermogravimetric analysis (TGA) within the temperature range of 30 ^{o}C to 1000 ^{o}C with a heating rate of 10 ^{o}C/min. The structural characterization of the prepared powder were performed with the help of X'Pert pro MPD XRD (PANalytical) X-ray diffractometer fitted with Cu Kα radiation (1.5406 Å). The morphological information of the samples were extracted using Carl Zeiss make Supra 35 VP field emission scanning electron microscope (FESEM) and microstructural characterizations were carried out using Tecnai G2 30ST (FEI) transmission electron microscope (TEM). Room temperature photoluminescence (PL) study was done using Horiba FluoroMax 4 spectrometer. The dye degradation experiment and light absorption capability of the sample were carried out with a UV–Vis spectrometer (CECIL Aquarius 7200).

2.4 Photocatalysis study

The photocatalytic study of doped and undoped BFO nanoparticles on organic dyes namely rhodamine b, methyl blue and bismarck brown were carried out using a UV-vis spectrometer under the illumination of normal visible light. In each experiment, 0.5 gm of catalyst were suspended in 100 ml of the aqueous solution made up of the different strong concentration of dyes (10 mg/l, 20 mg/l and 30 mg/l). Before any irradiation to visible light every time the suspension was kept in dark under constant stirring for 1 h. After this, the suspension is then irradiated with visible light under constant stirring for almost 1 h. During the whole process, 4 ml of suspension were collected and centrifuged at 10,000 rpm in a regular interval of time. Then the concentration of the solution was measured using a UV-vis spectrometer. And to

known the reusability of the sample, the whole suspension is centrifuged and washed properly to remove any leftover dye in it. Then the powder was dried and collected for reuse.

3. Results and discussion

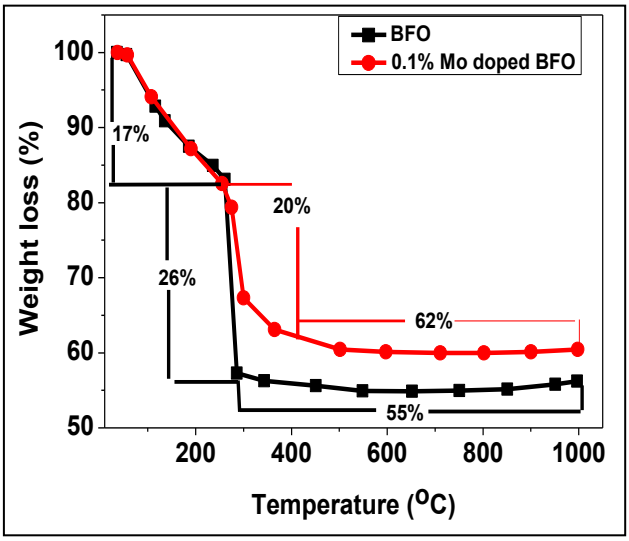

Figure 2 TGA measurements of BFO nanoparticles and 0.1% Mo-BFO doped nanoparticles for almost 1.30 h.

TGA analysis of the as-prepared sample is as shown in Figure 2. In first step, there is a weight loss of 17% in the temperature range of 30°C to 250°C for both the doped and undoped samples due to the loss of water. Afterwards, there is a second stage of weight loss for both the samples in the temperature range of 250°C to 400°C which may be attributed to the decaying of organic compound and release of nitrates. For the pure BFO sample, the weight loss is 26% and for 0.1 % doped BFO it is around 20%. There is a decrease in weight loss and an increase in residual yield [20]. No significant weight loss is observed and the curve becomes almost a straight line in the temperature range of 400°C to 1000°C indicating the samples can be calcined in any temperature above 400°C for the formation of BFO phase.

XRD patterns of all the samples calcined at 600 °C for 2 h are shown in Figure 3. All the peaks for BFO matched well with standard data (JCPDS No. 20-0169) which indicates

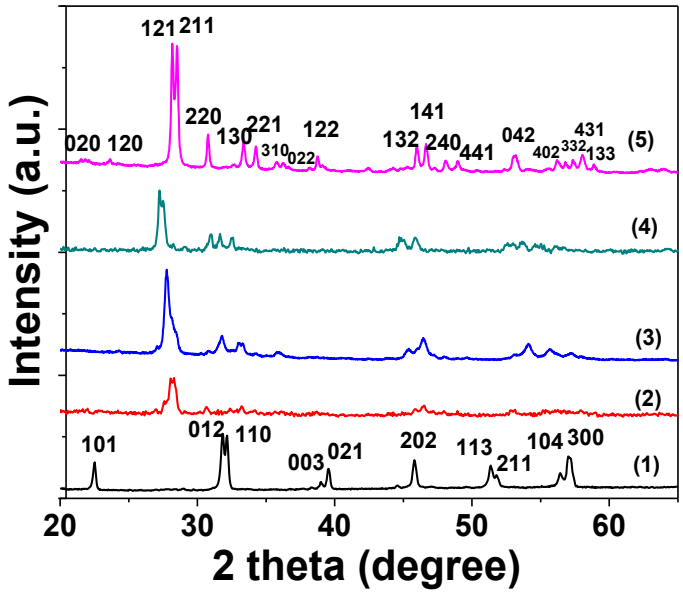

Figure 3 XRD patterns for the calcined samples (1) BFO (2) 0.025% Mo doped BFO (3) 0.05% Mo doped BFO (4) 0.075% Mo doped BFO (5) 0.1% Mo doped BFO.

the formation of pure BFO ($BiFeO_3$) phase. Interestingly, with the doping of Mo ions, it was observed that the $BiFeO_3$ phase begins to convert into second phase $Bi_2Fe_4O_9$ (JCPDS No.20-0836) and fully converted when the concentration of Mo reached 0.1%. So from the above observation, it was clear that the simple rhombohedral structure of $BiFeO_3$ completely converts to the orthorhombic structure on doping it with 0.1% Mo. A similar transformation of rhombohedral to orthorhombic for bismuth ferrite is reported elsewhere [9].

Table 1. BET analysis of the surface area, pore size and pore volume of the bismuth ferrite nanoparticle and 0.1% Mo doped bismuth ferrite nanoparticles.

Sample	**Surface area (m^2/g)**	**Pore volume (cc/g)**	**Pore radius (nm)**
BFO	4.383	0.045	3.113
0.1% Mo - BFO	7.777	0.045	3.113

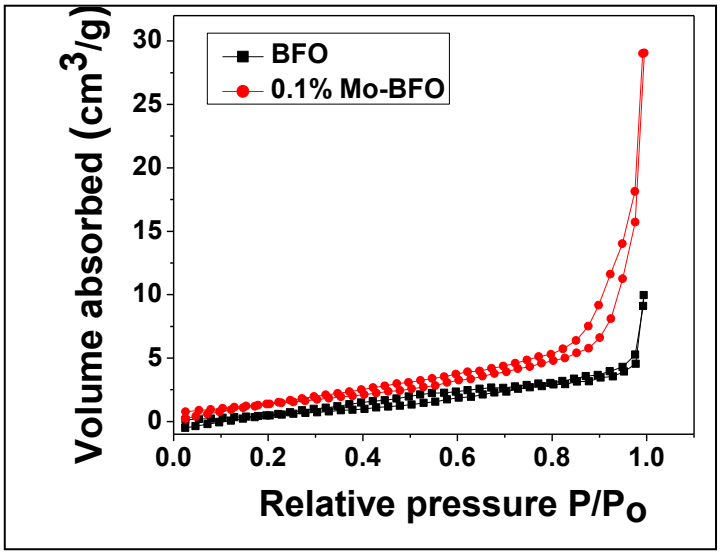

Figure 4 Nitrogen absorption/desorption isotherms of BFO and 0.1%-Mo doped BFO nanoparticles.

The BET surface area of BFO and 0.1% Mo-doped BFO nanoparticles are measured from N_2 absorption/desorption isotherm as shown in Figure 4. The pore size and pore volume are also given in Table 1. From the Table 1 it is clear that the surface area of bismuth ferrite nanoparticles increases on doping it with molybdenum ion. But the pore volume and pore radius remains almost the same. This increase in surface area may be due to the structural change occurs in the nanoparticles on doping.

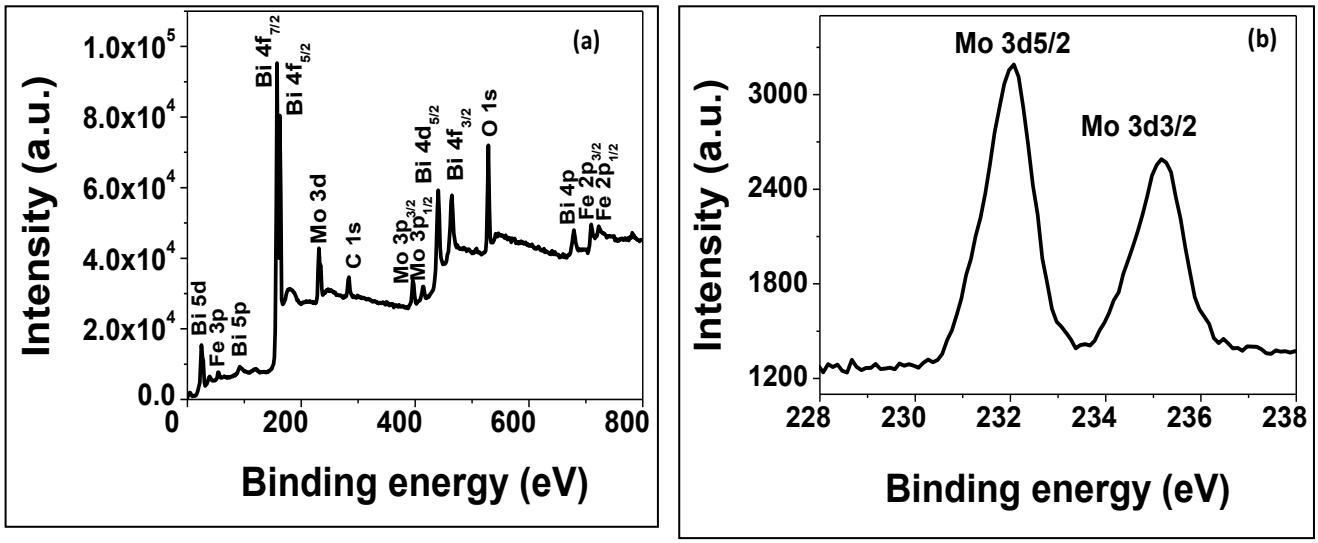

Figure 5(a) XPS spectra of 0.1%-Mo doped BFO nanoparticle, (b) High resolution spectra of Mo 3d core level.

X-ray photoelectron spectroscopy of 0.1% Mo-doped BFO nanoparticles is delineated in Figure 5(a). The peak at 530 eV corresponds to O 1s state of Mo-doped BFO nanoparticles. Doublet peaks at 158.85 eV and 164 eV corresponds to Bi $4f_{7/2}$ and $4f_{5/2}$ states respectively. There are prominent peaks from molybdenum of 3p and 3d states. Small peaks located at 398 eV and 414 eV are due to the presence of $3p_{3/2}$ and $3p_{1/2}$ state respectively in the sample. There is a sharp peak at 232 eV which corresponds to 3d oxidation state of Molybdenum. High-resolution core level spectra of 3d oxidation state of Molybdenum are carried out and two prominent peaks at 232 eV and 235 eV for Mo $3d_{5/2}$ and Mo $3d_{3/2}$, respectively are observed as shown in Figure 5(b). XPS study clearly delineates the presence of iron, bismuth, molybodinum and oxygen only and no impurity.

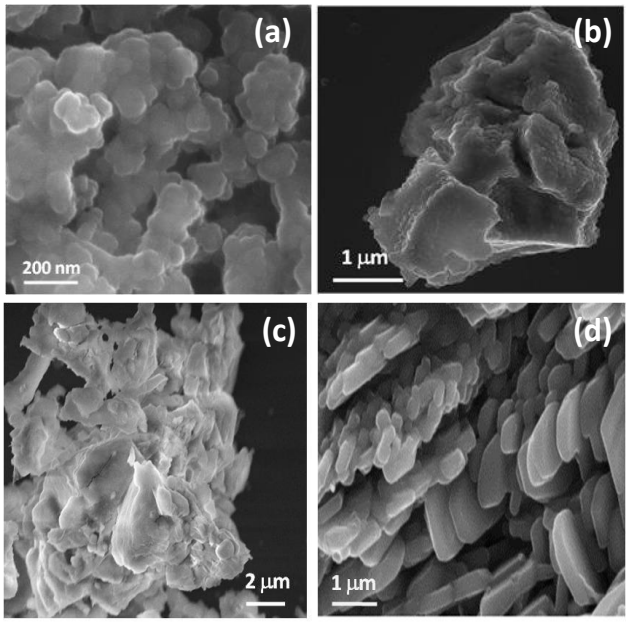

Figure 6 FESEM images of calcined samples at 600 ˚C (a) BFO, (b) 0.05% Mo –BFO, (c) 0.075% Mo-BFO, (d) 0.1% Mo –BFO.

Figure 6 shows the FESEM images of undoped and 0.1% Mo-doped BFO nanoparticles. From the above pictures, it is clearly observed that a morphological changefrom spherical to dedritic has occurred due to doping.

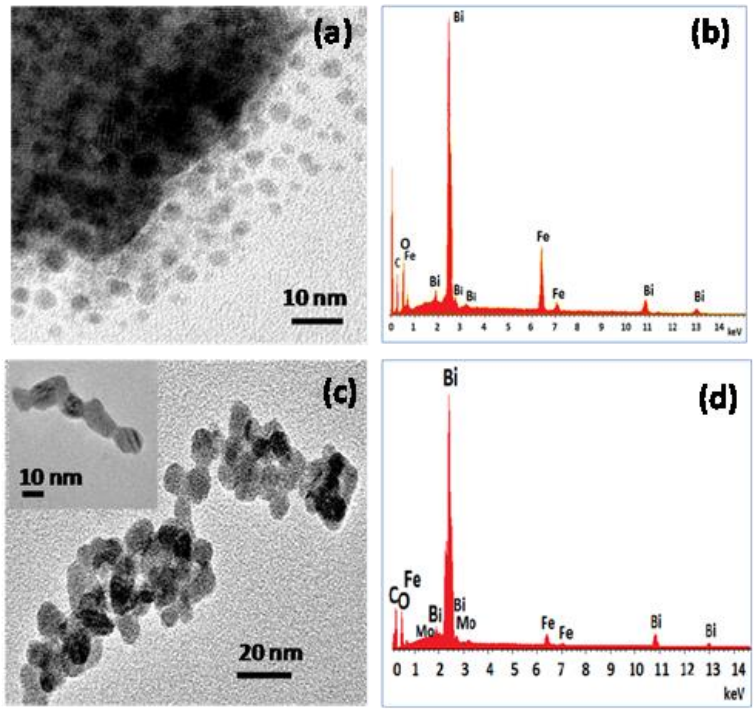

Figure 7 TEM images of samples calcined at 600 °C (a) BFO nanoparticles; (b) EDAX of BFO; (c) 0.1% Mo doped BFO; (d) EDAX of 0.1% Mo doped BFO.

The TEM micrographs of pure BFO and 0.1% Mo-doped BFO are presented in Figure 7(a) and Figure 7(c), respectively which delineates that both the samples contain a large number of almost spherical nanoparticles. Average particle size for BFO nanoparticles was found to be 7 nm (±1.8 nm) calculated from Figure 7(a). 0.1% Mo-doped BFOnanoparticles are larger than pure and the average size is around 15 nm as calculated from Figure 7(c). However, they are more agglomerated and looks like dendrite structure. Figure 7(b) and 7(d) shows the energy dispersive spectra (EDX) of both the samples. This spectrum again confirms that the samples contain no elements other than Bi, Fe, Mo, and O.

The influence of Mo doping on the energy band structure of BFO is investigated using UV-vis spectroscopy. The optical band gap of all the samples has been estimated by using the standard Tauc plot of absorption spectra as shown in Figure 8. Compared with the undoped one an efficient narrowing of bandgap for the 0.1% Mo-doped BFO sample was observed.

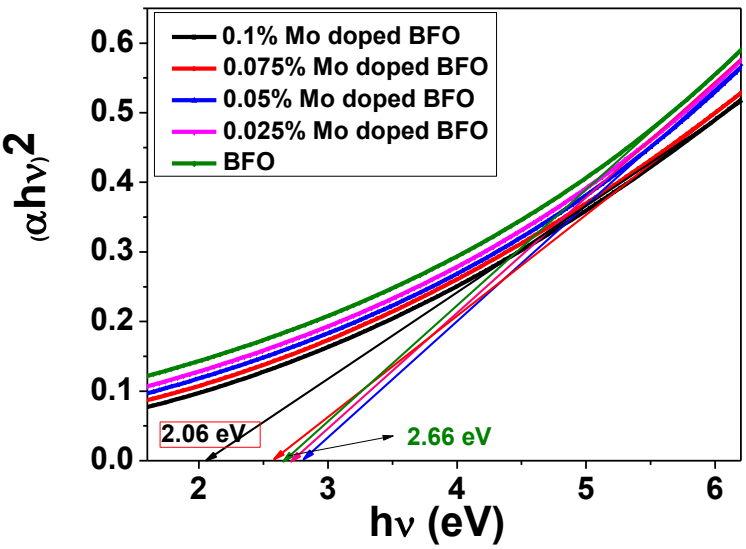

Figure 8 Concentration variation of the room-temperature UV−vis spectrum of the undoped and doped BFO nanoparticles.

The band gap for the undoped one is 2.66 eV which is higher than bulk BFO (2.2 eV). This increase of band gap may be attributed to the quantum size effect. Bandgap decreases to 2.01 eV for 0.1% Mo-doped BFO which leads to an increase in the absorption capability of the material and becomes a suitable photocatalytic agent. A decrease in bandgap on doping may be attributed to the increase of particle size which is clearly visible in TEM micrographs.

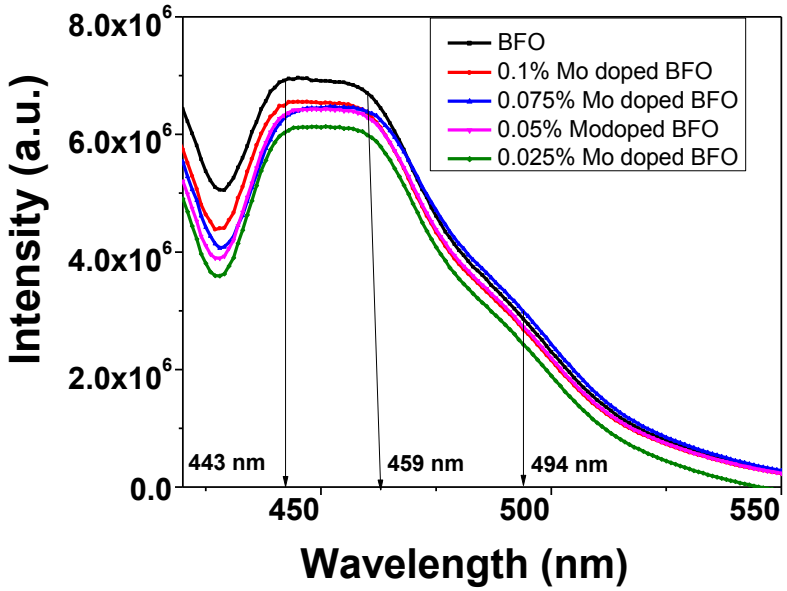

Figure 9 Concentration variations of the room-temperature PL spectra of the undoped and doped BFO nanoparticles.

Figure 9 shows the room temperature photoluminescence (PL) spectra of all the prepared samples. PL spectra of the samples show mainly three peaks at around 443 nm, 459 nm, and 492 nm while excited with 385 nm sources. Peaks around 443 nm may be attributed to the band-edge emission of BFO and the other two peaks are due to the oxygen vacancy defects states. It is evident from the figure that there was almost no shift in peak position but an effective change in intensity appears while doped with Mo ions. A constant decrease in intensity was observed as the doping percentage increases. This implies that the recombination rate is slower for the doped BFO which means that more photogenerated charge carriers will be available for dye degradation [21-23]. It is to be noted here that 0.1% Mo-doped BFO shows the lowest intensity among all other doped BFO nanoparticles. This shows that Mo doping enhances the sensitivity of BFO towards the visible light which in turns increases the efficiency of dye degradation.

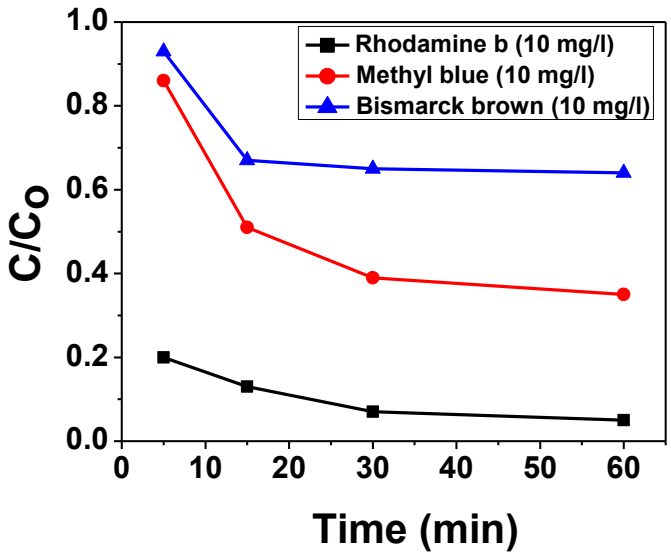

Figure 10 Photocatalytic degradation of Rhodamine b, methyl blue and bismarck brown as a function of the irradiation time under visible light for the as-prepared Mo-doped BFO samples.

The dye degradation process depends on different factors mainly absorption of photons, recombination of electron-hole pair and the catalytic effect of the sample [21, 24, 25]. Here we have observed an enhancement in photocatalytic dye degradation capability of nanocrystalline BFO on molybdenum doping. Photocatalytic properties of bismuth ferrite (BFO) nanoparticles both pure and Mo-doped under visible light ($\lambda > 400$ nm) irradiation are

explored for different organic dyes namely RhB, methyl blue, and bismarck brown. Mo-doped BFO nanoparticles show good results for all the mentioned dyes but among them, it shows maximum degradation for RhB as shown in Figure 10.

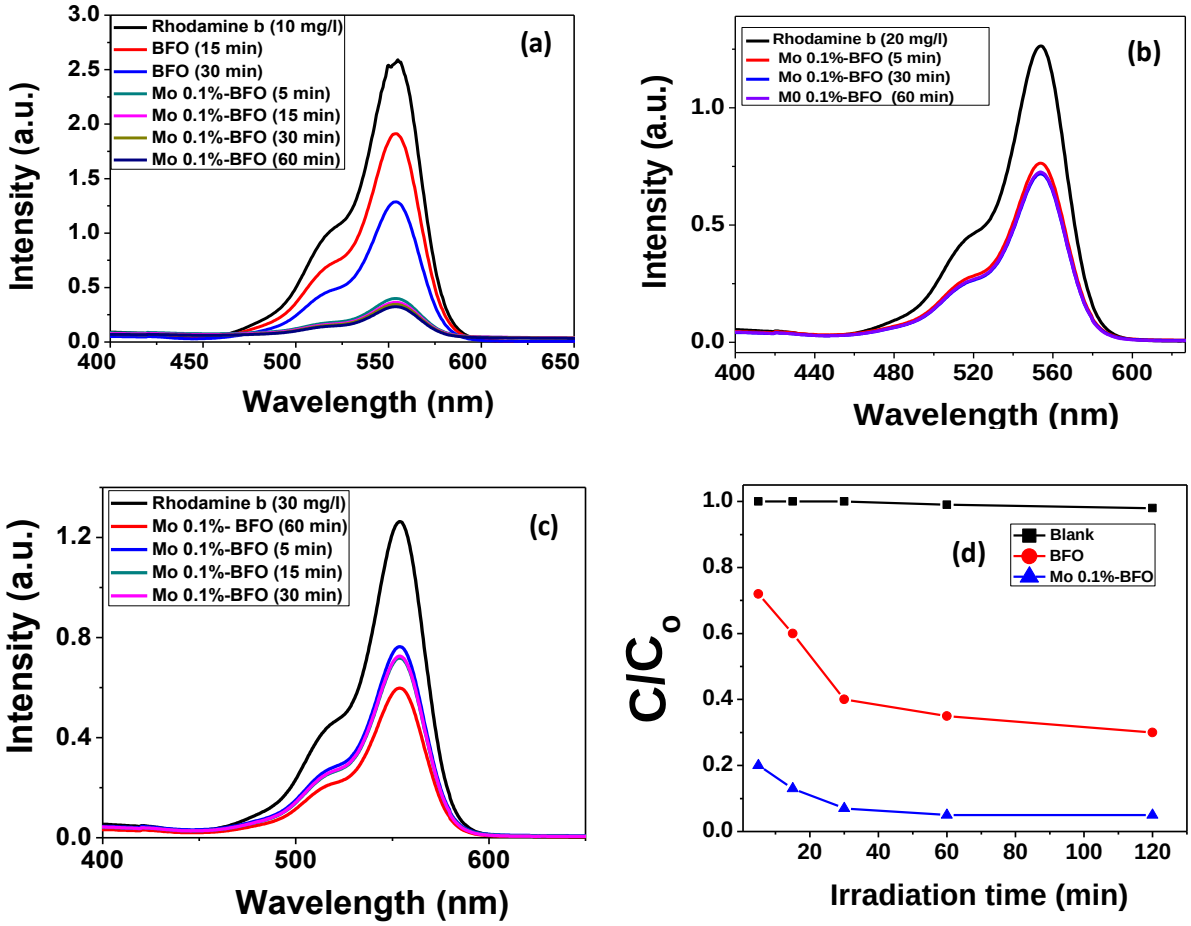

Figure 11 UV–vis absorption spectra of Rhodamine B (RhB) solution with undoped BFO and 0.1% Mo-doped BFO nanoparticles (a) 10 mg/l of RhB, (b) 20 mg/l of RhB, (c) 30 mg/l of RhB, (d) Photocatalytic degradation of Rhodamine b as a function of the irradiation time under visible light for the as-prepared Mo-doped BFO samples.

We have monitored the absorbance for different concentration of dyes (10 mg/l, 20 mg/l, and 30 mg/l) having 0.5 g per 100 ml of catalyst and kept it under vigorous stirring for almost 1 h in dark. Absorbance has been measured in visible light for different concentration as shown in Figure 11(a), 11(b), and 11(c). Degradation capability of all the pure and Mo-doped BFO (0.025%, 0.05%, 0.075%, 0.1%) samples have been checked for RhB. It is observed that among all the samples 0.1% doped Mo shows the highest photocatalytic activity. From the

time-dependent study shown in Figure 11(d) it is evident that the degradation rate is very fast. The dye degrades to almost 80% within 5 min of irradiations for 0.1% Mo-doped BFO samples. The enhanced catalytic effect of Mo-doped BFO towards RhB may be due to the fact that the doped sample has higher defect states confirmed from the photoluminescence spectra (Figure 9).

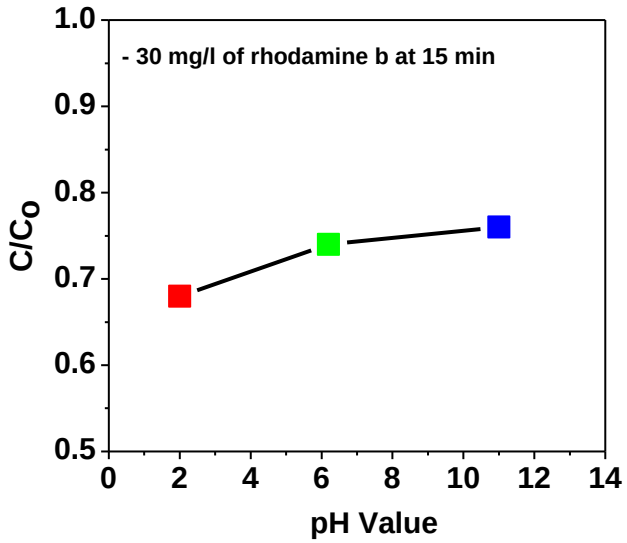

Figure 12 Photocatalytic degradation of RhB on 0.1%-Mo doped BFO nanoparticles at different pH.

Since the pH of the solution plays an important role in space charge properties of the dye, we have checked the pH dependency of the sample. Here we observed that photocatalytic activity of the prepared samples almost independent of pH as delineated in Figure 12 and so it can be used in any conditions.

To quantify the kinetics we have fitted the experimental data's with Langmuir–Hinshelwood model, which is expressed as below,

$$ln(\frac{C_o}{C}) = kt \quad (1)$$

Where C and C_o is the concentration of RhB after time t and t_o, k is the rate constant and t is the irradiation time.

The kinetics fits very well ($R^2 \sim 0.92$) for all the samples as shown in Figure 13. The rate constant of 0.1% Mo-doped BFO is the highest among all the samples. So this proves that

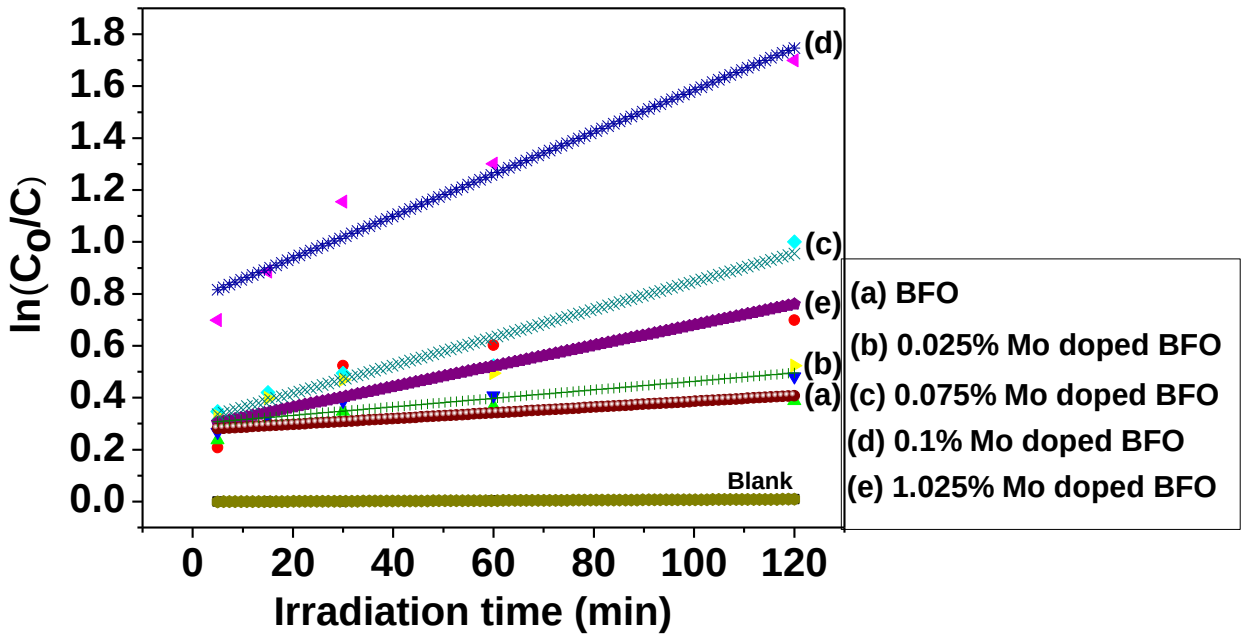

Figure 13 Psuedo first order kinitics fitting of BFO and Mo doped BFO samples.

0.1% doping of Mo in BFO enhances the dye degradation capacity of bismuth ferrite. There are several factors which could contribute to the dye degradation process. Achieved enhance and ultrafast dye degradation by Mo-doped BFO nanoparticles could be combined effect of three important factors. The structural change in bismuth ferrite nanoparticles due to Mo-doping will generate more defects as confirmed from PL study may contribute to dye degradation. Band gap narrowing is another issue which keeps the electron-hole separation more efficiently and contributes to dye degradation. In addition, molybdenum oxide itself is a good candidate for dye degradation. All together a synergistic effect of both molybdenum oxide and BFO is responsible for excellent performance.

Majority of the catalysts degrades dye while illuminating with UV light in presence of some promoter. As sunlight contains the maximum 4% UV component it could not be effectively used for dye degradation using such catalysts. The need of the hour is sustainable dye degradation process which can utilize sunlight available abundantly and works without any promoter like H_2O_2. Bismuth ferrite with a band gap of around 2.2 eV can be easily activated by visible light which has the capacity to degrade organic dyes including RhB though the rate is slow. Observed results delineate that there is a positive and pronounced effect of Mo ion doping on dye degradation capability of BFO. 80% degradation is achieved within five minutes of irradiation in visible light at normal ambient without any promoter. Therefore, Mo-doped BFO could be a promising catalyst which will be suitable for real application of dye degradation to clean industrial effluents very quickly, easily and inexpensively.

4. Conclusions

In summary, we have successfully synthesized molybdenum doped BFO nanoparticles using a simple chemical process. It is observed that doping of molybdenum increases the photocatalytic activity of BFO nanoparticles by four times under similar test condition. Molybdenum-doped BFO nanoparticles demonstrate more than 80% degradation capability for rhodamine-B (RhB) while illuminating it in visible light for five min under the ambient condition without any heating or H_2O_2. The effect of other parameters like concentration and

pH delineates that dye degradation process is independent of pH while doped with molybdenum. Additionally, prepared materials can also degrade other dyes like methylene blue and bismark brown very efficiently. Dye degradation as a whole an adsorption-oxidation-desorption process which is modified due to doping. The enhanced and ultrafast activity of molybdenum doped BFO nanoparticles could be a synergistic effect of BFO and molybdenum oxide. Demonstrated results show that it is possible to design very fast and highly efficient dye degradation system for various organic dyes to clean industrial effluents using ordinary light in ambient condition without any promoter.

Conflicts of interest

Author declares no conflict of financial interest.

Acknowledgements

SonamChakraborty is thankful to DST-INSPIRE for providing her fellowship (IF140385) and also to Material Characterization division of CSIR-CGCRI, Kolkata for rendering their support towards XRD, TEM /SEM measurements. Authors acknowledge M. Narjinary, Sk. Md. Mursalin, Md. JalaluddinMondal and Raju Manna for their help in making the sensor module and helping in measurement. The authors are also thankful to DST-CSIR Sensor Hub (GAP 0332) for providing the facilities to conduct our experiments.

References

[1] Zhao, X.; Dairong, C.; Abdul Q.; Chen, B.; Xiuling, J.; Beilstein J. Nanotechnol. 2017**,** 8, 2781–2789.

[2] Gao, T.; Chen, Z.; Niu, F.; Zhou, D.; Huang, Q.; Zhu, Y.; Qin, L.; Sun, X.; Huang, Y.; J. Alloys Compd. 2015, 648, 564-570.

[3] Yu, Y.; Wen, W.; Qian, X.; Liu, J.; Wu, J.; Sci. Rep. 2017, 7, 41253-41265.

[4] Yang, J.; C.; Chen, Ji, H.; Ma, W.; Zhao, J.; J. Phys Chem. B, 2005, 109, 21900-21907.

[5] Khomchenko, V. A.; Karpinsky, D. V.; Kholkin, A. L.; Sobolev, N. A.; Kakazei, G. N.; Araujo, J. P.; Troyanchuk, I. O.; Costa1, B. F. O.; Paixão, J. A.; J. Appl. Phys. 2010, 108, 74109-74114.

[6] Murcia-López, S.; Hidalgo, M. C.; Navío, J. A.; Appl. Catal A: Gen. 2012, 423–424, 34-41.

[7] Mandlimath, T. R.; Moliya, A.; Sathiyanarayanan, K. I.; Appl. Catal. A: Gen. 2016, 519, 34-47.

[8] Wang, Q.; Lian, J.; Ma, Q.; Bai, Y.; Tong, J.;Zhong, J.; Wang, R.; Huang, H.; Su, B.; New J. Chem. 2015, 39, 7112-7119.

[10] Peng,Y.; Chiou, S.; Hsiao, C.; Ouyang, C.; Tu, C.; Sci. Rep. 2017, 7, 45164-45172.

[11] Tiwari, D.; Fermin, D. J.; Chaudhuri, T. K.; Ray, A.; J. Phys. Chem. C, 2015, 119, 5872-5877.

[12] Chakraborty, S.; Pal, M.; New J. Chem. 2018, 42, 7188-7196.

[13] Das, R.; Khan, G. G.; Varma, S.; Mukherjee, G. D.; Mandal, K.; J. Phys. Chem. C , 2013, 117, 20209-20216.

[14] P. R. Vanga, R. V. Mangalaraja, M. Ashok, J. Mater. Sci. Mater. Electron.27 (2016) 5699-5706.

[15] N. Zhang, D. Chen, F. Niu, S. Wang, L. Qin, Y. Huang, Sci. Rep. 6 (2016) 26467-26477.

[16] Irfan, S.; Rizwan, S.; Shen, Y.; Li, L.; Asfandiyar, S.; Butt, C. W.; Nan, Sci. Rep. 2017, 7, 42493-42504.

[17] Sakar, M.; Balakumar, S.; Indranil, B.;Pradeep, K. G.; Sellamuthu, N. J.; RSC Adv. 2014, 4, 16871-16871.

[18] Yang, R.; Sun, H.; Li, J.; Li, Y.; Ceram. Int. 2018, 44, 14032-14035.

[19] Irfan, S.; Li, L.; Saleemi, A. S.; Nan, C. W.; J. Mater. Chem. A, 2017, 5, 11143-11151.

[20] Koao, L. F.; B. F.; Dejene, H. C. Swart, S. V. Motloung, T. E. Motaung, S. P. Hlangothi, Adv. Mater. Lett. 2016, 7, 529-535.

[21] Li, Y. F.; Xu, D.; Oh, J.; Shen, W.; Li, X.; Yu, Y.; ACS Catal. 2012, 2, 391-398.

[22] Bharathkumar, S.; Sakar, M.; Balakumar, S.; J. Phys. Chem. C, 2016, 120, 18811-18821.

[23] Hauser, A.; Zhang, J.; Mier, J. L.; Ricciardo, R. A.; Woodward, P. M.; Gustafson, T. L.; Brillson, L. J.; Yang, F. Y.; Appl. Phys. Lett. 2008, 92, 222901-222903.

[24] Zhang, Q.; Gong, W.; Wang, J.; Ning, X.; Wang, Z.; Zhao, X.; Ren, W.; Zhang, Z.; J. Phys. Chem. C, 2011, 115, 25241-25246.

[25] Merupo, V. I.; Velumani, S.; Oza, G.; Makowska-Janusik, M.; Kassiba, A.; Mater. Sci.Semicond.Process. 2015, 31, 618-623.